


SPECIAL ISSUE ARTICLE

WILEY

Bashkirian taeniate bisaccate pollen-dominated palynological assemblage from northwestern Junggar Basin, Xinjiang Province, China

Tianming Shi¹ | Qiong Li¹ | Aliya Amuti¹ | Jinan Xiao¹ | Feng Liu² |
Wan Yang³ | Qiuli Li⁴ | Hua Zhang² | Zeng Lü⁵ | Huiping Peng² 

¹Research Institute of Experiment and Detection of Xinjiang Oilfield Company, Xinjiang, China

²State Key Laboratory of Palaeobiology and Stratigraphy, Nanjing Institute of Geology and Palaeontology and Center for Excellence in Life and Palaeoenvironment, Nanjing, China

³Geology and Geophysics Program, Missouri University of Science and Technology, Rolla, Missouri

⁴State Key Laboratory of Lithospheric Evolution, Institute of Geology and Geophysics, Chinese Academy of Sciences, Beijing, China

⁵The Key Laboratory of Orogenic Belts and Crustal Evolution, Ministry of Education, School of Earth and Space Sciences, Peking University, Beijing, China

Correspondence

Huiping Peng, State Key Laboratory of Palaeobiology and Stratigraphy, Nanjing Institute of Geology and Palaeontology and Center for Excellence in Life and Palaeoenvironment, Nanjing 210008, China.
Email: hppeng@nigpas.ac.cn

Funding information

The Second Tibetan Plateau Scientific Expedition and Research, Grant/Award Number: 2019QZKK0706; National Natural Science Foundation of China, Grant/Award Numbers: 41372011, 41530101, 41530103; The Strategic Priority Research Program (B) of the CAS, Grant/Award Number: XDB03010103; The US National Science Foundation (Wan Yang), Grant/Award Number: EAR 1714749

Handling Editor: Z.-Q. Chen

The Early Pennsylvanian land plant community is characterized by widespread forests consisting of lycopsids, ferns, and seeds fern in swampy wetlands. The contemporaneous palynological assemblages are mainly composed of spores of *Lycospora* spp., *Densosporites* spp., and *Laevigatosporites* spp. and monosaccate prepollen of *Florinites* spp. Taeniate bisaccate pollen appeared for the first time during the Early Pennsylvanian but never prevailed in the coeval palynological assemblages. Here, we report a taeniate bisaccate pollen-dominated palynological assemblage from the Jiamuhe Formation of Well Ke 85 in the Zhongguai Uplift, northwestern Junggar Basin, Xinjiang. Nineteen miospore species belonging to 14 genera were identified from the assemblage. Based on their relative abundance, one assemblage is nominated informally as *Calamospora breviradiata*–*Lunatisporites tersus* (BT) assemblage. SIMS U–Pb geochronological analysis of zircons from two volcanic ash beds from the basal and upper parts of the formation yields weighted mean $^{206}\text{Pb}/^{238}\text{U}$ dates of 316.3 ± 2.2 Ma (MSWD = 1.2, $n = 19$) and 316.5 ± 2.8 Ma (MSWD = 0.85, $n = 20$) in an ascending order. A Bashkirian age is thus assigned to the BT assemblage. Our combined palynological and geochronological investigations reveal an early stage of the rise of conifers in the Kazakhstan Plate and offer a rare glimpse into the Early Pennsylvanian land vegetation in the subtropical area at the northern hemisphere.

KEYWORDS

Carboniferous, Jiamuhe Formation, Junggar Basin, Pennsylvanian, zircon U–Pb geochronology

1 | INTRODUCTION

Uplift in the northwestern part of the basin has been an important oil-producing region (Yuan et al., 2020) and is speculated to contain The Junggar Basin is a large petroliferous basin in north Xinjiang, abundant Carboniferous gas reservoirs (Hu et al., 2020; Figure 1). The China (Cao et al., 2020; Zhang, Jin, Lan, & Zhao, 2015). The Zhongguai Jiamuhe Formation is one of the most promising target intervals in

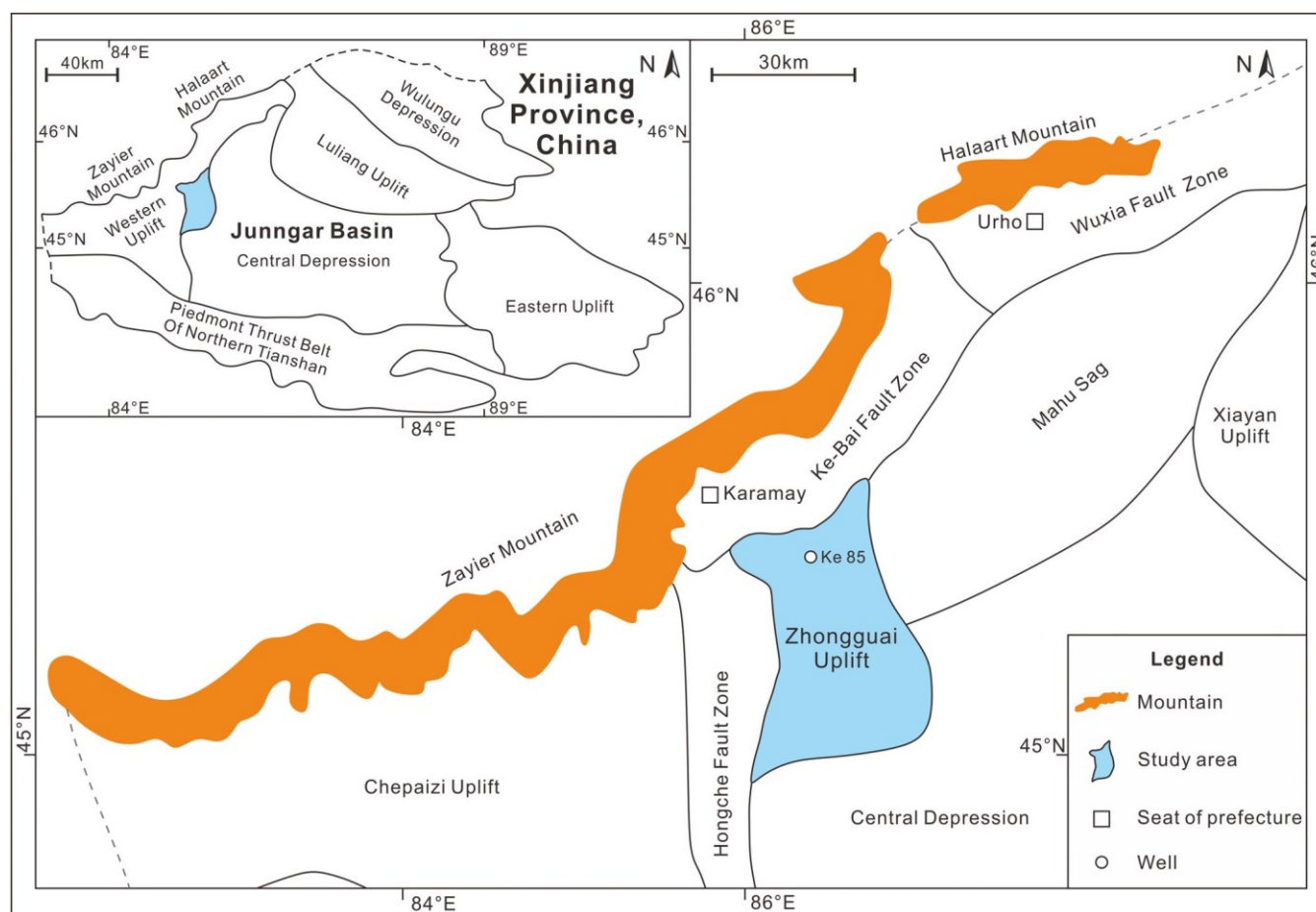


FIGURE 1 Tectonic map showing the location of Junggar Basin (inset) and Zhongguai Uplift. Well Ke 85 is located in northern Zhongguai Uplift in northwestern Junggar Basin, Xinjiang Province, China [Colour figure can be viewed at wileyonlinelibrary.com]

the Zhongguai Uplift and mainly consists of conglomerates and basic-intermediate igneous rocks. In the last two decades, a tremendous amount of study has been conducted on the stratigraphic correlation of the formation (Li et al., 2018; Liang, He, Wu, Lu, & Zhang, 2018). However, due to the lack of age constraints by index marine invertebrate fossils and radioisotopic ages, there remain great uncertainties on the age and stratigraphic subdivision of the formation. Palynological investigations on limited dark grey siltstone and claystone in the subsurface and outcropped Jiamuhe Formation have revealed a consistent gymnosperm striate pollen-dominated palynological assemblage showing a typical 'Permian' appearance (Ouyang, Wang, Zhan, & Zhou, 2003). Thus, the formation has been considered to have an early Permian age (Li, Xu, Liu, Wang, & Xiang, 2016).

Here, we present palynological and chronological findings from the Jiamuhe Formation of Well Ke 85 in Zhongguai Uplift, northwestern Junggar Basin, Xinjiang. The palynological data provide a foundation for stratigraphic correlation of Jiamuhe Formation in the subsurface and offer new insights into land-plant community changeovers associated with the Early Pennsylvanian environmental changes in the Kazakhstan Plate.

2 | GEOLOGICAL SETTING

The Junggar Basin is surrounded by Palaeozoic deformed subduction assemblage complexes, including the Halaart, Zayier and Chepaizi mountains in the northwest, Qinggelidi and Karamaili mountains in the northeast and Tianshan in the south (Sengör, Natal'in, Sunal, & Voo, 2018; Figure 1). Tectonically, the Junggar Block is located in the convergent area of Kazakhstan, Siberian and Tarim plates. From the Carboniferous to Neogene, the basin had gone through various tectonic phases, viz. rift, foreland, intraplate, and reactivated foreland basins (Wang & Chen, 2004).

Zhongguai Uplift is at the northwest margin of Junggar Basin, as a petroliferous tectonic unit. Its north margin is bordered by the NE–SW-striking Ke-Bai fault zone, which belongs to a thrust belt formed by lateral compression and basement uplift (Chen, 2019; Figure 1). The west margin of the uplift is confined by the N-S-striking Hongche fault zone and can be divided into an area of thrust faults in the north and a segment of strike-slip faults in the south in map view or separated into the lower part of compressional faults and upper part of extensional faults in a cross-sectional view (Wu et al., 2019). The south margin of the Zhongguai Uplift is demarcated by thrust faults, while its eastern margin is bordered by the Mahu Sag and Central Depression (Wu et al., 2017; Zhang, Gao, Zhang, Yu, & Du, 2018).

The stratotype section of the Jiamuhe Formation is in the southern part of Halaart Mountains, about 90 km north of Zhongguai Uplift (Zhang & Wu, 1991). Seismic data show that the formation dips into the Zhongguai Uplift in the subsurface and is subdivided into three units based on the proportion of igneous rocks. Well Ke 85 is located in the north part of Zhongguai Uplift (Figure 1). It penetrates the lower part of Jiamuhe Formation in the Zhongguai Uplift with a thickness of 323.4 m, which consists of black shale in the lower part, coarse sandstone intercalated with conglomerate in the middle part, and maroon and purple siltstone with common calcite-filled vugs in the upper part (Figure 2). The black shale is finely laminated, seemingly monotonic, and intercalated with siltstone and very fine sandstone laminae. Abundant plant fossil seeds, leaves, and barks, mainly *Mesocalamites* spp. in prints, are concentrated on bedding planes, locally as carbonaceous laminae (Figure 3z). It is interpreted to be deposited in a swamp environment on a coast plain or flood plain. The conglomerate in the middle part consists of fine, moderately well-sorted, angular to subrounded pebbles and granules as thin beds and lenses, 1–5 cm thick. It is clast-supported with an erosional base. The clasts are dominantly andesite. The sandstone is moderately well-sorted, angular to subangular, and well planar or tabular cross-bedded. This interval is interpreted as deposits in a braided stream environment. The upper part of Jiamuhe Formation in Well Ke 85 starts from 15 cm of fine-pebble conglomerate at the base, overlain by 3.5 m of thick-laminated siltstone with common calcite-filled vugs, which are 1–10 mm in diameter as possible root moulds. The upper part is interpreted as a pedogenically altered meandering stream deposit (Figure 2).

Sampling for palynology focused on dark siltstone and claystone in Well Ke 85. In total, 26 cleaned core samples were crushed, weighed (30–50 g for each sample), and treated with standard HCl-HF-HCl palynological maceration (Wood, Gabriel, & Lawson, 1996). The organic residues were sieved through 180 and 10 μm meshes. The residues were then mounted on permanent microscope slides using glycerin jelly. Only two samples from the depth of 3,097 and 3,417 m, respectively, contain palynomorphs (Figure 2). Palynomorphs were observed and photographed with a LEICA DM 2500 microscope and D800E camera. All slides are stored in the State Key Laboratory of Palaeobiology and Stratigraphy, Nanjing Institute of Geology and Palaeontology, Chinese Academy of Sciences, Nanjing, China, under specimen numbers Ke 85-11-3417 and Ke 85-12-3097. All spores and pollen in the figures are located by using an England Finder Slide.

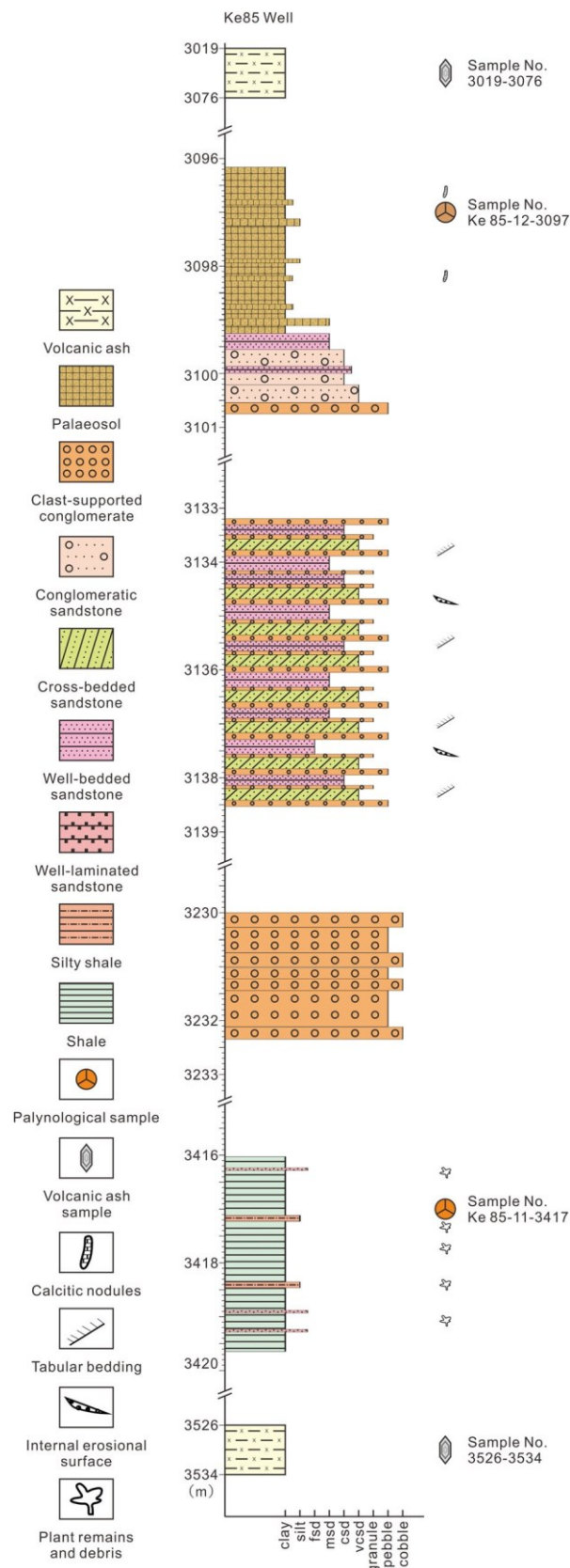


FIGURE 2 Lithostratigraphy of Jiamuhe Formation in Well Ke 85, showing the location of rock samples for palynological and

geochronological analyses [Colour figure can be viewed at wileyonlinelibrary.com]



FIGURE 3 Legend on next page.

Zircons were separated from the two samples (about 2 g each) through standard magnetic and density separation procedures. The size of zircon grains varies between 150 and 20 μm , and the shape is euhedral prismatic or anhedral rounded to subhedral (Figure 4). Zircon grains and zircon standards Plešovice and Qinghu were mounted in a transparent epoxy disk and polished away about 1/3 of crystals for analyses. All zircons were observed under transmitted and reflected light photo-microscopy and cathodoluminescence (CL) imaging to identify suitable domains for analyses (Figure 4; Rubatto & Gebauer, 2000). The mount was vacuumcoated with high-purity gold before SIMS measurements. U, Th, and Pb isotopes were measured by CAMECA IMS 1280 SIMS at the Institute of Geology and Geophysics, Chinese Academy of Sciences (IGGCAS) in Beijing. The monocollector mode was adapted to collecting isotopic data, and each measurement consists of seven cycles with a total analytical time of ca. 12 min. During the analyses, the primary O_2 ion beam was accelerated at 13 kV, with an intensity of ca. 8 nA and an analysis spot size of 20 μm 30 μm . The detailed analytical procedure has been described by Li, Liu, Li, Guo, and Chamberlain (2009) and Li et al. (2010). Analyses of zircon standards were interspersed with unknown grains. U-Th-Pb ratios and absolute abundances were determined relative to the standard Plešovice (Slama et al., 2008) and the standard 91500 (Wiedenbeck et al., 1995), respectively. Non-radiogenic ^{204}Pb was used to correct the common Pb. The corrections are sufficiently small to be insensitive to the choice of common Pb composition. An average of present-day crustal Pb composition (Stacey & Kramers, 1975) was used for the common Pb, assuming that the common Pb is largely surface contamination introduced during sample preparation. The age calculations and plotting of Concordia diagrams were made using ISOPLOT (Ludwig, 2012).

4 | PALYNOLOGICAL ASSEMBLAGE

Two productive samples from the depths of 3,097 and 3,417 m of Well Ke 85 yield a similar palynological assemblage. Trilete spores (40–43%) and pollen (57–60%) play roughly equal roles in the assemblage (Table 1). Trilete spores exhibit a relatively low genetic diversity and are characterized by the dominance of *Calamospora breviradiata* (32–32.33%)

and *Calamospora hartungiana* (7.3–10%) with the rare occurrence of *Granulatisporites crenulatus* (0–1%) and *Leiotriletes* spp. (0–0.67%). Pollen mainly consists of taeniate and non-taeniate forms. Taeniate pollen accounts for a larger percentage (40.33–42.67%) of the assemblage and is characterized by *Lunatisporites tersus* (15.67–18%), *Illinites hiatus* (9.33–14.33%), *Protohaploxypinus* spp. (4.67–8%), and *Striatolebachiites ellipticus* (5.33–6%) with rare occurrences (<5%) of *Striatomonosaccites orientalis* and *Hamiapollenites* sp. Non-taeniate pollen is a subordinate component (14.33–19.33%) of the assemblage and mainly composed of *Gardenasporites comitatus* (8.33–11%) and *Falcisporites sublevis* (3–7.67%) with rare occurrences (<1.5%) of *Florinites luberae*, *Cordaitina annulata*, and *Platysaccus papilionis*. Because of the overwhelming dominance of *Calamospora breviradiata* and *Lunatisporites tersus*, the assemblage is nominated informally as *Calamospora breviradiata*–*Lunatisporites tersus* (BT) assemblage.

The BT assemblage is characterized by a roughly equal proportion between triete spores and pollen. A similar palynological composition has been observed in the palynological assemblage recovered from the Dongtujinhe Group in the Sugursu section and Liushugou Formation in the Qijiagou section (Zhou, 1994). The common occurrence of *Calamospora hartungiana* in these two palynological assemblages also supports the palynological correlation with the BT assemblage. However, the palynological assemblage of Dongtujinhe Group and Liushugou Formation differs in its rare appearance of taeniate bisaccate pollen (<5%; Zhou, 1994). The *Calamospora liquida*–*Striatoabieites rugosus* (LR) Biozone proposed by Ouyang et al. (2003) in the Tashikula Formation at the southern margin of Junggar Basin is also characterized by frequent occurrence of *Calamospora breviradiata* and *C. hartungiana*, as well as an equal proportion of trilete spores and pollen. It indicates a palynological correlation between LR Biozone and BT assemblage. However, all chronostratigraphic investigations on the Tashikula Formation so far have consistently pointed to an early Permian age (Gao et al., 2020).

5 | CHRONOSTRATIGRAPHY

Zircons in two side cores from depths of 3,019–3,076 m and 3,526–3,534 m of Well Ke 85 were dated by SIMS. To verify the

FIGURE 3 Selected palynomorphs and plant remains recovered from Jiamuhe Formation in Well Ke 85. Palynomorphs specimens are identified by Ke 85-sample number-well depth-slide number; miospore locations on slides are indicated by England Finder coordinates (EF). Scale bar = 50 μm , except where specified. (a) *Leiotriletes* spp. Ke 85-11-3417-1, EF: U38/4. (b) *Granulatisporites crenulatus* Playford, 1964. Ke 85-12-3097-1, EF: O40/3. (c and d) *Calamospora breviradiata* Kosanke, 1950. (c) Ke 85-12-3097-2, EF: H42; (d) Ke 85-11-3417-1, EF: R41. (e) *Calamospora hartungiana* Schopf, in Schopf, Wilson and Bentall, 1944. Ke 85-11-3417-1, EF: V39. (f) *Florinites luberae* Samoilovich, 1953. Ke 85-11-3417-1, EF: R47/4. (g) *Cordaitina annulata* Inosova et al., 1976. Ke 85-11-3417-1, EF: Q39/4. (h) *Striatolebachiites ellipticus* Wang, 2003. Ke 85-11-3,417-1, EF: K42/3. (i) *Striatomonosaccites orientalis* Wang, 2003. Ke 85-11-3417-1, EF: S42/2. (j and k) *Illinites*? *hiatus* Ouyang, 2003.

(j) Ke 85-12-3097-2, EF: H44; (k) Slide Ke 85-11-3417-1, EF: T50/4. (l–n) *Lunatisporites tersus* Ouyang, 2003. (l) Ke 85-12-3097-1, EF: K41/2; (m) Ke 85-12-3097-1, EF: H39; (n) Ke 85-11-3417-1, EF: S51. (o and p) *Gardenasporites comitatus* Ouyang, 2003. (o) Ke 85-11-3417-1, EF: R45/3; (p) Ke 85-12-3097-1, EF: J44/2–1. (q–s) *Protohaploxylinus perfectus* (Naumova ex Kara-Murza) Samoilovich, 1953. (q) Ke 85-11-3,417-1: N35/4; (r) Ke 85-12-3097-2, EF: U39/2; (s) Ke 85-11-3417-1, EF: L46/4. (t) *P. arachnoideus* Zhan, 2003. Ke 85-11-3417-1, EF: T38/4. (u) *P. chalonerii* Clarke, 1965. Ke 85-12-3097-2, EF: L32. (v) *P. samoilovichiae* (Jansonius) Hart, 1964. Ke 85-11-3417-1, EF: L37/2. (w) *Hamiapollenites* spp. Ke 85-12-3097-1, EF: H40. (x) *Platysaccus papilionis* Potonié and Klaus, 1954. Ke 85-11-3417-1, EF: U39/2. (y) *Falcisporites sublevis* Ouyang and Norris, 1999. Ke 85-11-3417-1, EF: S42. (z) *Mesocalamites* spp. Ke 85-3417 [Colour figure can be viewed at wileyonlinelibrary.com]

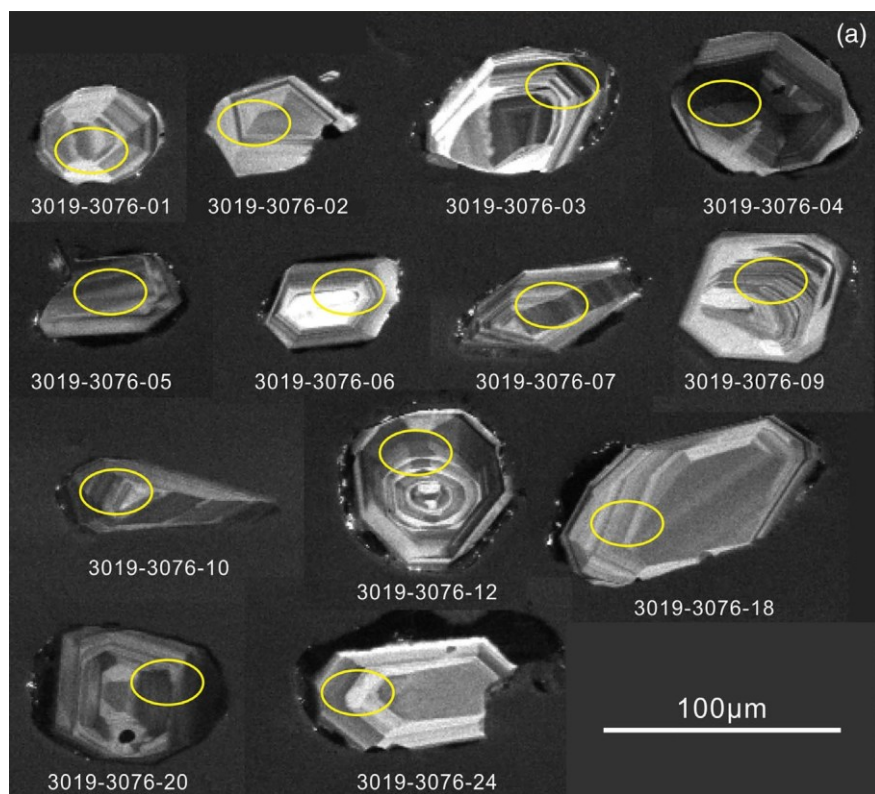


FIGURE 4 Cathodoluminescence images of selected zircons analysed by the in-situ U–Pb SIMS technique. The yellow ellipses show the analysed areas and are approximately 20–30 µm in size. Each number under a zircon grain corresponds to the analysis number in Table 2 [Colour figure can be viewed at wileyonlinelibrary.com]

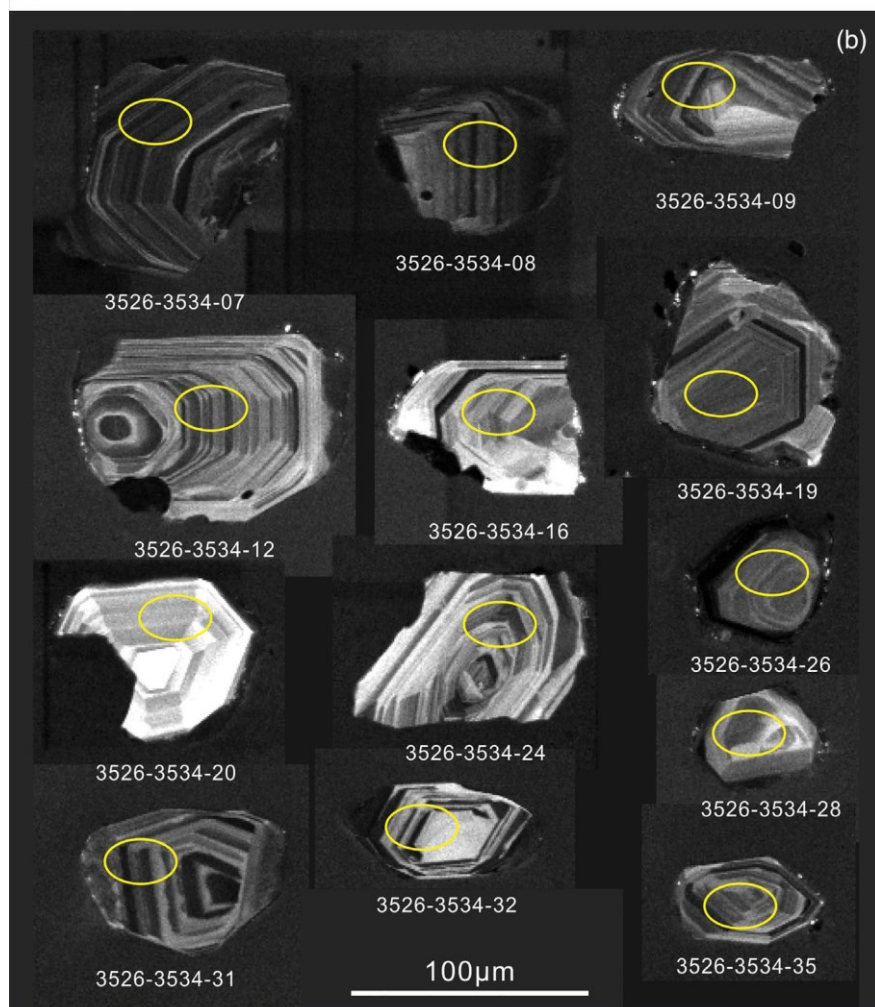


TABLE 1 Statistical data based on counts of 300 grains in each sample and relative abundance of miospore species recovered from Jiamuhe Formation of Well Ke 85

Spores and pollen taxa	Species	Number		Percentages (%)	
		Ke-85-12-3097	Ke-85-11-3417	Ke-85-12-3097	Ke-85-11-3417
Spores	Leiotriletes spp.		2		0.67
	Granulatisporites crenulatus Playford, 1964	3		1.00	
	Calamospora breviradiata Kosanke, 1950	96	97	32.00	32.33
	Calamospora hartungiana Schopf, in Schopf, Wilson and Bentall, 1944	30	22	10.00	7.33
Non-taeniate species	Florinites luberae Samoilovich, 1953	1	2	0.33	0.67 1.33
	Cordaitina annulata Inosova et al., 1976		4		
	Falcisporites sublevis Ouyang and Norris, 1999	9	23	3.00	7.67
	Platysaccus papilionis Potonié and Klaus, 1954		4		1.33
	Gardenasporites comitatus Ouyang, 2003	33	25	11.00	8.33
Taeniate species	Striatomonosaccites orientalis Wang, 2003	1	4	0.33	1.33
	Striatolebachiites ellipticus Wang, 2003	16	18	5.33	6.00
	Illinites? hiatus Ouyang, 2003	43	28	14.33	9.33
	Lunatisporites tersus Ouyang, 2003	54	47	18.00	15.67
	Protohaploxypinus perfectus (Naumova ex Kara-Murza) Samoilovich, 1953	6	11	2.00	3.67
	P. arachnoideus Zhan, 2003		4		1.33
	P. chaloneri Clarke, 1965	2	1	0.67	0.33
	P. samoilovichiae (Jansonius) Hart, 1964	4	7	1.33	2.33
	Hamiapollenites spp.	2	1	0.67	0.33

external uncertainties of SIMS U–Pb zircon dating calibrated against the Plešovice standard, a Qinghu standard was alternately analysed as an unknown. Fourteen analyses on Qinghu zircons produced a Concordia age of 160.7 ± 1.1 Ma (MSWD = 0.94, $n = 14$; Table 2), which is within the error range of the recommended ID-TIMS value of 159.5 ± 0.2 Ma (Li et al., 2013). The error ellipses and bars of the zircon dates are 2σ in the plots (Figure 5).

Sample 3,019–3,076 was collected from the side core at the top of the Well Ke 85 (Figure 2). Zircons from this sample are mostly euhedral to subhedral and 20 to 150 μm in length with length–width ratios ranging from 1.5 to 4. CL images show that most of the zircons exhibit oscillatory zoning indicative of a magmatic origin (Figure 4; Corfu, Hanchar, Hoskin, & Kinny, 2003; Zeck & Williams, 2002). Thirty-three analyses were done on 33 zircons (Table 2). U and Th contents span from 82 to 1,087 and 50 to 1,028 ppm, respectively. Th/U ratios are ca. 0.4 to 1.6 and show a moderately positive relationship between the contents of Th and U. Apart from the nine analyses with a high content of common Pb, the f_{206} value (i.e., proportion of common ^{206}Pb in total measured ^{206}Pb) is lower than 1.80%. Fourteen zircons are likely detrital zircons, and the other 19 analyses give

indistinguishable $^{206}\text{Pb}/^{238}\text{U}$ ratios within analytical uncertainties with a weighted mean $^{206}\text{Pb}/^{238}\text{U}$ date of 316.5 ± 2.8 Ma (MSWD = 0.85, $n = 19$, 95% confidence interval; Figure 5).

Sample 3,526–3,534 was collected from the side core at the base of Well Ke 85 (Figure 2). Most zircons in this sample are euhedral to subhedral. The grains are 20–160 μm in length and have a length–width ratio ranging from 1.1 to 5. The oscillatory zoning of the zircons under CL (Figure 4), together with the Th/U ratios varying from ca. 0.2 to 1.2 (Table 2), indicates a magmatic origin (Corfu et al., 2003; Rubatto & Gebauer, 2000; Zeck & Williams, 2002). U and Th contents vary from 52 to 4,067 and 39 to 2,078 ppm, respectively. Thirty analyses were carried out on 30 zircons (Table 2). Apart from the 11 analyses with a high content of common Pb, the f_{206} values are lower than 1.29%. Ten zircons are likely detrital zircons, and the other 20 analyses give indistinguishable $^{206}\text{Pb}/^{238}\text{U}$ ratios within analytical uncertainties with a weighted mean $^{206}\text{Pb}/^{238}\text{U}$ date of 316.3 ± 2.2 Ma (MSWD = 1.2, $n = 20$, 95% confidence interval; Figure 5).

6 | DISCUSSIONS

A distinct vegetation changeover from a pteridophyte-dominated to seed-plant-dominated flora has been recognized in the

Carboniferous–Permian transitional palaeobotany and palynology, representing by replacing older plants, such as *Cordaite*s, *Calamites*, and

Lepidodendron, by conifers, such as various members of the *Voltziales* in Laurasia, and glossopterids in Gondwana (Traverse, 2007). Because most taeniate bisaccate pollen has been proved to be produced by conifer and glossopterids, its dominance in palynological assemblages, as a signature of the times to come in seed-plant-

TABLE 2 SIMS zircon U–Pb data for two volcanic ash samples and the Qinghu zircon standard. The data in italics are probably produced by detrital zircons and not used for age calculation

Sample/spot	[U] ppm	[Th] ppm	Th/U meas	²³⁸ U — ²⁰⁶ Pb	±σ %	²⁰⁷ Pb — ²⁰⁶ Pb	±σ %	Age (Ma)	±σ
3,019–3,076-02	334	166	0.498	19.355	1.53	0.09865	1.15	305.9	4.8
3,019–3,076-31	239	203	0.850	20.330	1.54	0.05318	1.57	309.3	4.7
3,019–3,076-09	338	248	0.733	19.748	1.51	0.07356	1.26	310.0	4.7
3,019–3,076-05	192	151	0.786	19.986	1.55	0.06392	1.75	310.3	4.8
3,019–3,076-10	166	88	0.530	19.263	1.65	0.08467	1.74	313.1	5.2
3,019–3,076-19	231	112	0.485	20.059	1.54	0.05252	1.77	313.7	4.8
3,019–3,076-01	186	143	0.771	18.100	1.60	0.12659	1.88	314.5	5.5
3,019–3,076-24	90	134	1.484	19.944	1.57	0.05366	2.47	315.0	4.9
3,019–3,076-20	246	269	1.095	19.517	1.56	0.06927	2.13	315.4	4.9
3,019–3,076-04	324	403	1.245	19.869	1.53	0.05482	1.56	315.7	4.8
3,019–3,076-18	216	196	0.909	19.765	1.56	0.05313	2.65	318.0	4.9
3,019–3,076-12	319	109	0.341	19.170	1.50	0.07616	2.82	318.2	4.8
3,019–3,076-06	206	88	0.425	19.740	1.57	0.05171	2.04	319.0	5.0
3,019–3,076-03	174	101	0.581	19.692	1.54	0.05296	2.27	319.3	4.9
3,019–3,076-07	388	602	1.553	19.666	1.53	0.05374	1.33	319.4	4.8
3,019–3,076-08	715	1,028	1.438	19.560	1.51	0.05789	1.17	319.4	4.8
3,019–3,076-15	106	75	0.708	18.574	1.59	0.09331	5.69	320.9	5.6
3,019–3,076-11	256	124	0.487	19.429	1.54	0.05512	1.66	322.6	4.9
3,019–3,076-17	299	240	0.801	19.175	1.54	0.05319	1.69	327.6	5.0
3,019–3,076-13	273	208	0.762	18.648	1.55	0.06158	1.49	333.1	5.1
3,019–3,076-32	109	67	0.619	18.775	1.56	0.05138	2.23	335.3	5.2
3,019–3,076-33	487	245	0.502	18.643	1.57	0.05476	1.38	336.2	5.2
3,019–3,076-30	250	122	0.491	18.548	1.53	0.05450	1.50	338.0	5.1

3,019–3,076-21	371	208	0.561	18.336	1.52	0.06024	1.39	339.3	5.1
3,019–3,076-27	1,083	396	0.366	18.521	1.51	0.05243	0.68	339.3	5.0
3,019–3,076-26	210	123	0.586	18.346	1.51	0.05457	1.65	341.6	5.1
3,019–3,076-34	230	63	0.273	18.344	1.62	0.05278	1.49	342.4	5.5
3,019–3,076-23	82	50	0.608	18.164	1.73	0.05374	2.57	345.3	5.9
3,019–3,076-29	313	266	0.849	17.946	1.53	0.05431	1.27	349.2	5.2
3,019–3,076-22	278	239	0.858	17.933	1.52	0.05441	1.35	349.4	5.2
3,019–3,076-25	278	223	0.804	17.920	1.52	0.05298	1.53	350.3	5.3
3,019–3,076-14	111	88	0.788	17.650	1.58	0.05419	2.40	355.0	5.6
3,019–3,076-28	170	99	0.582	16.726	1.53	0.05449	1.81	374.1	5.6
3,526–3,534-34	4,067	2078	0.511	20.655	1.52	0.05332	0.39	304.4	4.6
3,526–3,534-21	189	220	1.165	20.287	1.55	0.05449	1.90	309.4	4.7
3,526–3,534-05	340	153	0.451	20.225	1.53	0.05507	1.42	310.1	4.7
3,526–3,534-36	1,211	625	0.516	20.200	1.51	0.05318	0.67	311.3	4.6
3,526–3,534-16	95	74	0.780	20.217	1.59	0.05220	2.70	311.4	4.9
3,526–3,534-24	276	108	0.390	20.145	1.53	0.05311	1.42	312.1	4.7
3,526–3,534-28	52	39	0.749	19.991	1.63	0.05760	4.17	312.7	5.1
3,526–3,534-12	126	58	0.460	19.945	1.71	0.05934	3.31	312.7	5.3
3,526–3,534-19	255	236	0.927	19.809	1.55	0.05326	1.66	317.3	4.9
3,526–3,534-20	108	62	0.575	19.585	1.58	0.05740	2.87	319.2	5.0
3,526–3,534-26	982	520	0.529	19.673	1.53	0.05388	1.05	319.2	4.8
3,526–3,534-08	118	99	0.836	19.619	1.58	0.05563	2.41	319.3	5.0

TABLE 2 (Continued)

	[U] ppm	[Th] ppm	Th/U meas	²³⁸ U	±σ %	²⁰⁷ Pb	±σ %		
Sample/spot				²⁰⁶ Pb		²⁰⁶ Pb		Age (Ma)	±σ
3,526–3,534-07	208	134	0.646	19.656	1.53	0.05315	2.30	319.7	4.8
3,526–3,534-32	247	163	0.659	19.571	1.53	0.05492	1.46	320.4	4.8
3,526–3,534-35	239	105	0.438	19.557	1.58	0.05490	1.68	320.6	5.0
3,526–3,534-09	513	440	0.857	19.355	1.51	0.06271	1.05	320.7	4.8
3,526–3,534-31	245	126	0.516	19.585	1.57	0.05349	1.68	320.8	5.0
3,526–3,534-10	411	306	0.747	19.430	1.50	0.05958	1.38	320.8	4.8
3,526–3,534-17	298	136	0.457	19.409	1.53	0.05259	1.49	324.0	4.9
3,526–3,534-03	527	472	0.896	19.191	1.55	0.06096	1.69	324.1	5.0
3,526–3,534-06	176	79	0.445	18.895	1.58	0.06507	1.78	327.4	5.1
3,526–3,534-11	520	113	0.217	18.879	1.64	0.05773	1.31	330.8	5.3
3,526–3,534-15	226	132	0.583	18.868	1.51	0.05483	1.82	332.2	4.9
3,526–3,534-01	1,302	500	0.384	18.892	1.50	0.05302	0.88	332.5	4.9
3,526–3,534-30	248	134	0.538	18.551	1.51	0.05253	1.51	338.8	5.1

3,526–3,534-23	1,057	806	0.762	17.893	1.93	0.05312	0.91	350.7	6.7
3,526–3,534-04	204	70	0.341	14.780	1.55	0.09955	1.73	398.3	6.3
3,526–3,534-29	195	103	0.530	15.148	1.51	0.05496	1.79	412.1	6.1
3,526–3,534-27	446	322	0.722	12.022	1.51	0.05742	0.85	515.2	7.6
3,526–3,534-13	211	155	0.736	7.132	1.53	0.07042	0.95	842.4	12.6
Qinghu-1	1,241	667	0.538	40.217	1.65	0.04815	1.13	158.5	2.6
Qinghu-2	1,652	355	0.215	39.645	1.52	0.04807	0.98	160.8	2.4
Qinghu-3	642	312	0.486	40.077	1.52	0.04845	1.79	159.0	2.4
Qinghu-4	1,424	599	0.421	39.602	1.51	0.05084	1.05	160.4	2.4
Qinghu-5	1,042	402	0.386	40.578	1.57	0.04864	1.41	157.0	2.4
Qinghu-6	1,284	712	0.554	39.868	1.52	0.04939	1.07	159.7	2.4
Qinghu-7	879	374	0.426	39.966	1.53	0.04918	1.30	159.3	2.4
Qinghu-8	2,079	1,091	0.525	39.079	1.53	0.04966	0.87	162.8	2.5
Qinghu-9	1,788	963	0.539	39.408	1.90	0.04941	0.95	161.5	3.0
Qinghu-10	1,485	803	0.541	39.786	1.54	0.04944	1.42	160.0	2.4
Qinghu-11	1,396	638	0.457	39.539	1.52	0.04971	1.21	160.9	2.4
Qinghu-12	1,790	1,013	0.566	39.055	1.59	0.04926	1.05	163.0	2.6
Qinghu-13	991	359	0.362	39.234	1.56	0.04965	1.62	162.2	2.5
Qinghu-14	3,870	634	0.164	38.726	1.50	0.04941	0.89	164.3	2.4

Note: The data in italics are probably produced by detrital zircons and are not used for age calculation.

Abbreviation: SIMS, secondary ion mass spectrometry.

dominated flora which had gradually replaced the former wetland floras, is an event of global significance. Following the broad pattern of the development from monosaccate to bisaccate and non-taeniate to taeniate pollen, the taeniate bisaccate pollen was generally considered to have its first appearance and rapid increase in abundance during the Early Permian (Balme, 1980; Kemp et al., 1977; Loboziak & Clayton, 1988). However, recent palynological investigations in Xinjiang Province, China, have revealed a diachronous pattern of the evolution of non-taeniate and taeniate bisaccate pollen (Ouyang, 1996; Zhou, 1994). The earlier known pollen-dominated palynomorph assemblages, which occur in Dongtujinhe Group and Qijiagou Formation in the Tianshan in northwestern China, were described and illustrated by Zhou (1994). The Bashkirian–Moscovian ages of these assemblages were documented from co-occurring marine fossils, such as fusulinid *Millerella* and ammonoid *Reticuloceras* (Liao et al., 1990). More than half of the palynomorphs recovered from Dongtujinhe Group and Qijiagou Formation are saccate pollen grains with non-taeniate predominating over less common taeniate forms. The palynological

assemblage recovered by Ouyang, Zhou, Wang, & Zhan, 1994 from the equivalent Batamayineishan Formation in Junggar Basin is characterized by the first appearance of taeniate bisaccate pollen and the predominance of non-taeniate bisaccate pollen. This assemblage was named *Noeggerathiopsidozonotrites varicus* *Striatolebachiites junggarensis* (VJ) Assemblage and assigned a Bashkirian age on the independent evidence of brachiopods and ostracods (Ouyang et al. (1994)). These palynological assemblages from the Junggar Basin resemble the BT assemblage described herein and is correlative to the early bisaccate pollen-dominated assemblages from the Ettrain equivalents of the Yukon Territory (Barss, 1972), the Late Bashkirian–Early Moscovian Otto Fiord Formation on Ellesmere Island, Arctic (Utting, 1985), and the Moscovian Serginsk Formation in central Urals (Dyupina, 1979). It suggests that conifer or conifer-like gymnosperms flourished much earlier in northern subtropical areas than in other parts of Pangea. The Junggar Basin appears to have the earliest known communities of conifer or conifer-like gymnosperms. This early appearance of the drought-tolerant plant community was attributed

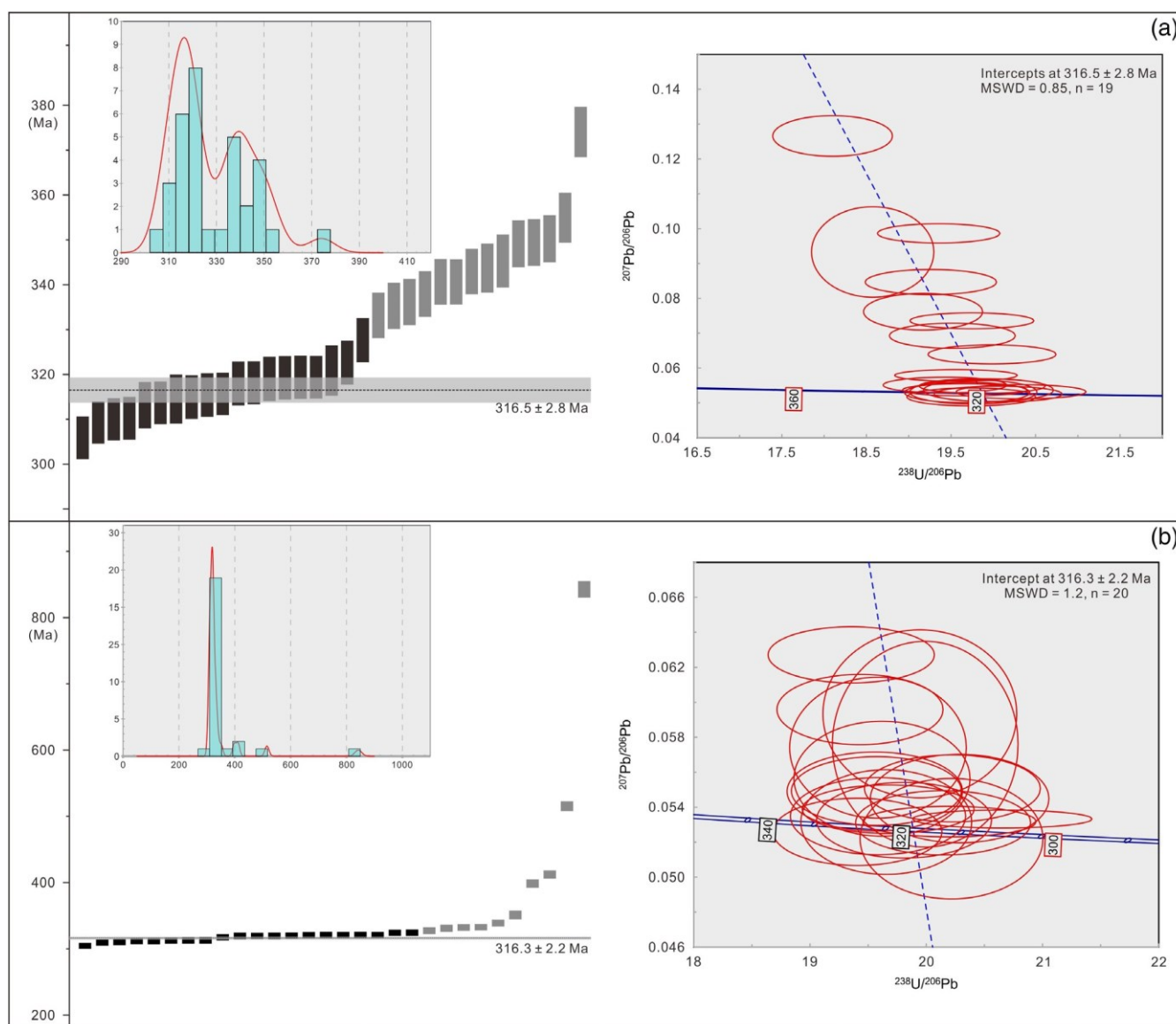


FIGURE 5 Date distribution plots of sample 3,019–3,076 (a) and sample 3,526–3,534 (b) in Well Ke 85. Vertical bars represent the $^{206}\text{Pb}/^{238}\text{U}$

$\text{Pb}/^{238}\text{U}$ date and 2σ analytical uncertainty of individual zircon analyses; the youngest group data (solid bars) are used for age calculation. Horizontal lines and shaded bands specify the calculated weighted mean dates and their 2σ uncertainties, respectively. Concordia plots correspond to SIMS analyses only. See Table 2 for complete U–Pb data [Colour figure can be viewed at wileyonlinelibrary.com]

to seasonally xeric environments in northern subtropical areas during the Bashkirian (Zhou, 1994). However, the BT assemblage described herein differs from these contemporaneous palynological assemblages by the dominance of taeniate bisaccate pollen. It indicates that taeniate bisaccate pollen should have first occurred before the Bashkirian, which is paralleled with the first appearance of non-taeniate bisaccate pollen (Owens, 1996). Thus, the general lineages from bisaccate and non-taeniate to taeniate pollen should be reevaluated. Palaeozoic taeniate bisaccate pollen has been widely considered to be yielded by Glossopteridales, an order of seed ferns from Gondwana (Pant & Nautiyal, 1960; Taylor, 1988). However, it has been demonstrated that it could come from conifers in the northern hemisphere (Clement-Westerhof, 1974). Loboziak and Clayton (1988) recorded an early appearance of taeniate bisaccate pollen, including Illinites, Protohaploxypinus, and Strotosporites, in upper Gzelian sediments. It was attributed to the increasing influence of the Gondwana component in the Euramerican palynoflora following the closure of the Rheic Ocean (Nance et al., 2012). The BT assemblage from the northwestern Junggar Basin predates these assemblages, indicating that the Carboniferous-Permian taeniate bisaccate pollen in the northern hemisphere may not have much to do with the subsequent history of taeniate bisaccate pollen in Gondwana, or taeniate bisaccate pollen may have evolved in parallel more than once. Thus, the BT assemblage indicates a potential new approach to the phylogeny of early conifers. Interestingly, this early appearance of taeniate bisaccate pollen-dominated palynological assemblage in the northwestern Junggar Basin coincides with the Bashkirian glacial maximum of the Late Palaeozoic Ice Age (LPIA; Chen et al., 2016). Although the changeover of land plant community from pteridophyte-dominated to seed-plant-dominated attached more to the drying trend after LPIA (DiMichele, Bashforth, Falcon-Lang, & Lucas, 2020; DiMichele, Montañez, Poulsen, & Tabor, 2009), land vegetation in the subtropical region of the northern hemisphere probably took the lead in entering into seed-plant-dominated floras due to the seasonally dry climate driven by the Bashkirian glacial maximum of LPIA.

7 | CONCLUSIONS

A taeniate bisaccate pollen-dominated assemblage from the lowest Pennsylvanian in Well Ke 85 cores provides insight into late Palaeozoic plant development in the Kazakhstan Plate. The following conclusions can be drawn from this study:

1. A taeniate bisaccate pollen-dominated microflora appeared in the Bashkirian of the northwestern Junggar Basin. This age is well constrained by radio-isotopic ages dated by the secondary ion mass spectrometry (SIMS) U–Pb zircon technique from two volcanic ash samples of Well Ke 85.
2. The first appearance of taeniate bisaccate pollen in the Junggar Basin is much earlier than that in other phytogeographic provinces and paralleled the first appearance of bisaccate non-taeniate pollen. It

indicates a potential new approach to early conifer phylogeny in the subtropical areas of the northern hemisphere.

ACKNOWLEDGEMENTS

The authors thank Limei Feng for her help in sample maceration, and Yu Liu, Xiaoxiao Ling, Jiao Li, and Hongxia Ma for their assistance during SIMS analyses. The authors are grateful to Dr. Mingli Wan for his assistance on plant fossil identification. This work was funded by the Second Tibetan Plateau Scientific Expedition and Research (2019QZKK0706), Youth Innovation Promotion Association of the Chinese Academy of Sciences (CAS) for Feng Liu, the Strategic Priority Research Program (B) of the CAS (grant XDB03010103), the National Natural Science Foundation of China (grants 41530103, 41530101, and 41372011) and Project of PetroChina Xinjiang Oilfield Company (grants 2019-c4032). Wan Yang is partially supported by the US National Science Foundation (EAR 1714749).

PEER REVIEW

The peer review history for this article is available at <https://publons.com/publon/10.1002/gj.4167>.

DATA AVAILABILITY STATEMENT

The data that support the findings of this study are available from the corresponding author upon reasonable request.

ORCID

Huiping Peng  <https://orcid.org/0000-0002-9024-0280>

REFERENCES

- Balme, B. E. (1980). Palynology and the Carboniferous-Permian boundary in Australia and other Gondwana continents. *Palynology*, 4(1), 43–55.
- Barss, M. (1972). A problem in Pennsylvanian – Permian palynology of Yukon territory. *Geoscience and Man*, 4(1), 67–71.
- Cao, J., Xia, L., Wang, T., Zhi, D., Tang, Y., & Li, W. (2020). An alkaline lake in the Late Paleozoic Ice Age (LPIA): A review and new insights into paleoenvironment and petroleum geology. *Earth-Science Reviews*, 202, 103091.
- Chen, B., Joachimski, M. M., Wang, X., Shen, S., Qi, Y., & Qie, W. (2016). Ice volume and paleoclimate history of the Late Paleozoic Ice Age from conodont apatite oxygen isotopes from Naqing (Guizhou, China). *Palaeogeography, Palaeoclimatology, Palaeoecology*, 448, 151–161.
- Chen, J. (2019). Squeezing reverse fault physical experiment and new explanation of Ke-Bai Fault Zone factor. *Journal of Jiangnan Petroleum University of Staff and Workers*, 32(1), 9–12.
- Clement-Westerhof, J. A. (1974). In situ pollen from gymnospermous cones from the Upper Permian of the Italian Alps – A preliminary account. *Review of Palaeobotany and Palynology*, 17(1–2), 63–73.
- Corfu, F., Hanchar, J. M., Hoskin, P. W., & Kinny, P. (2003). Atlas of zircon textures. *Reviews in Mineralogy and Geochemistry*, 53(1), 469–500.
- DiMichele, W. A., Bashforth, A. R., Falcon-Lang, H. J., & Lucas, S. G. (2020). Uplands, lowlands, and climate: Taphonomic megabiases and the apparent rise of a xeromorphic, drought-tolerant flora during the Pennsylvanian-Permian transition. *Palaeogeography, Palaeoclimatology, Palaeoecology*, 559, 109965.

- DiMichele, W. A., Montañez, I., Poulsen, C., & Tabor, N. J. (2009). Climate and vegetational regime shifts in the Late Paleozoic ice age earth. *Geobiology*, 7(2), 200–226.
- Dyupina, G. V. (1979). Palynological characteristics of Moscovian state of western Urals. In G. N. Papulov & I. V. Pakhomov (Eds.), *Typical Carboniferous Sections of Urals (Opornii Rasresi Karbona Urala)* (Vol. 141, pp. 67–84). Moskva, USSR: Trans. Inst. Geol. Geochem.
- Gao, Y., Huang, H., Tao, H., Carroll, A. R., Qin, J., Chen, J., ... Wang, C. (2020). Paleoenvironmental setting, mechanism and consequence of massive organic carbon burial in the Permian Junggar Basin, NW China. *Journal of Asian Earth Sciences*, 194, 104222. <https://doi.org/10.1016/j.jseae.2019.104222>.
- Hu, S., Wang, X., Cao, Z., Li, J., Gong, D., & Xu, Y. (2020). Formation conditions and exploration direction of large and medium gas reservoirs in the Junggar Basin, NW China. *Petroleum Exploration and Development*, 47(2), 266–279.
- Kemp, E. M., Balme, B. E., Helby, R. J., Kyle, R. A., Playford, G., & Price, P. L. (1977). Carboniferous and Permian palynostratigraphy in Australia and Antarctica: A review. *BMR Journal of Australian Geology and Geophysics*, 2(3), 177–208.
- Li, H., Tang, H., Qin, Q., Fan, C., Han, S., Yang, C., & Zhong, C. (2018). Reservoir characteristics and hydrocarbon accumulation of Carboniferous volcanic weathered crust of Zhongguai high area in the western Junggar Basin, China. *Journal of Central South University*, 25(11), 2785–2801.
- Li, Q., Li, X., Liu, Y., Tang, G., Yang, J., & Zhu, W. (2010). Precise U–Pb and Pb–Pb dating of Phanerozoic baddeleyite by SIMS with oxygen flooding technique. *Journal of Analytical Atomic Spectrometry*, 25(7), 1107–1113.
- Li, X., Liu, Y., Li, Q., Guo, C., & Chamberlain, K. R. (2009). Precise determination of Phanerozoic zircon Pb/Pb age by multicollector SIMS without external standardization. *Geochemistry, Geophysics, Geosystems*, 10 (4), Q04010.
- Li, X., Tang, G., Gong, B., Yang, Y., Hou, K., Hu, Z., ... Li, W. (2013). Qinghu zircon: A working reference for microbeam analysis of U–Pb age and Hf and O isotopes. *Chinese Science Bulletin*, 58(36), 4647–4654.
- Li, Y., Xu, Q., Liu, J., Wang, R., & Xiang, K. (2016). Redefinition and geological significance of Jiamuhe Formation in Hala'ate Mountain of West Junggar, Xinjiang. *Earth Science-Journal of China University of Geosciences*, 41(9), 1479–1488.
- Liang, Y., He, D., Wu, S., Lu, Y., & Zhang, L. (2018). The geometry, kinematics of Hong-3 well eastern fault and its structural model. *Chinese Journal of Geology*, 53(2), 420–433. <https://doi.org/10.12017/dzjx.2018.023>.
- Liao, Z., Wang, Y., Jiang, N., Wang, K., Liao, W., Ouyang, S., ... Li, S. (1990). Carboniferous stratigraphy. In Z.-T. Liao, W.-H. Yang, & Z.-L. Wei (Eds.), *Report of carboniferous and its ore possibility of Northern Xinjiang* (pp. 8–143). Urumchi, Xinjiang: Xinjiang Uyfur Autonomous Region.
- Loboziak, S., & Clayton, G. (1988). The Carboniferous palynostratigraphy of northeast Libya. In: A. El-Arnauti, B. Owens, B. Thusu (Eds.), *Subsurface Palynostratigraphy of Northeast Libya*, (pp. 129–149). Benghazi: Garyounis University/Agoco/CIMP.
- Ludwig, K. R. (2012). *Isoplot 3.75. A geochronological toolkit for Microsoft Excel* (p. 75). Berkeley, CA: Berkeley Geochronology Center.
- Nance, R. D., Gutiérrez-Alonso, G., Keppie, J. D., Linnemann, U., Murphy, J. B., Quesada, C., ... Woodcock, N. H. (2012). A brief history of the Rheic Ocean. *Geoscience Frontiers*, 3(2), 125–135. <https://doi.org/10.1016/j.gsf.2011.11.008>.
- Ouyang, S. (1996). On the first appearance of some gymnospermous pollen and GSPD assemblages in the Sub-Angara, Euramerian and Cathaysia provinces. *Palaeobotanist*, 45, 20–32.
- Ouyang, S., Wang, Z., Zhan, J., & Zhou, Y. (2003). *Palynology of the Carboniferous and Permian Strata of Northern Xinjiang, Northwestern China* (pp. 1–700). Hefei, Anhui: University of Science and Technology of China Press.
- Ouyang, S., Zhou, Y., Wang, Z., & Zhan, J. (1994). On occurrence of palynological assemblages of gymnospermous, specially striate pollen dominance (GSPD) from Bashikirian-Moscovian sediments in northern Xinjiang, NW. China. *Acta Palaeontologica Sinica*, 33(1), 24–47.
- Owens, B. (1996). Upper Carboniferous spores and pollen. In J. Jansonius & D. C. McGregor (Eds.), *Palynology: Principles and application* (Vol. 2, pp. 594–606). Salt Lake City, UT: Publisher Press.
- Pant, D. D., & Nautiyal, D. D. (1960). Some seeds and sporangia of *Glossopteris* flora from Raniganj Coalfield, India. *Palaeontographica Abteilung B*, 107, 41–64.
- Rubatto, D., & Gebauer, D. (2000). Use of cathodoluminescence for U–Pb zircon dating by ion microprobe: Some examples from the Western Alps. In *Cathodoluminescence in Geosciences* (pp. 373–400). Berlin, Heidelberg: Springer.
- Sengör, A. M. C., Natal'in, B. A., Sunal, G., & Voo, R. V. D. (2018). The tectonics of the Altaids: Crustal growth during the construction of the continental lithosphere of Central Asia between 750 and 130 Ma ago. *Annual Review of Earth and Planetary Sciences*, 46(1), 439–494. <https://doi.org/10.1146/annurev-earth-060313-054826>.
- Slama, J., Košler, J., Condon, D. J., Crowley, J. L., Gerdes, A., Hanchar, J. M., ... Norberg, N. (2008). Plešovice zircon – A new natural reference material for U–Pb and Hf isotopic microanalysis. *Chemical Geology*, 249(1–2), 1–35.
- Stacey, J. t., & Kramers, J. (1975). Approximation of terrestrial lead isotope evolution by a two-stage model. *Earth and Planetary Science Letters*, 26 (2), 207–221.
- Taylor, T. N. (1988). Pollen and pollen organs of fossil gymnosperms: Phylogeny and reproductive biology. In C. B. Beck (Ed.), *Origin and evolution of gymnosperms* (pp. 177–217). New York, NY: Columbia University Press.
- Traverse, A. (2007). Carboniferous/Permian Palynology to the end of the "Paleophytic". In N. H. Landman & D. S. Jonges (Eds.), *Paleopalynology* (pp. 229–273). Dordrecht: Springer.
- Utting, J. (1985). Palynomorphs from the type section of the Otto Fiord Formation (Upper Carboniferous) on Ellesmere Island, Queen Elizabeth Islands, Canada. *Bulletin of Canadian Petroleum Geology*, 33(3), 341–349.
- Wang, W., & Chen, Y. (2004). Tectonic evolution and petroleum systems in the Junggar Basin. *Acta Geologica Sinica-English Edition*, 78(3), 667–675.
- Wiedenbeck, M., Alle, P., Corfu, F. y., Griffin, W. L., Meier, M., Oberli, F. v., ... Spiegel, W. (1995). Three natural zircon standards for U–Th–Pb, LuHf, trace element and REE analyses. *Geostandards Newsletter*, 19(1), 1–23.
- Wood, G. D., Gabriel, A. M., & Lawson, J. C. (1996). Palynological techniques-processing and microscopy. In J. Jansonius & D. C. McGregor (Eds.), *Palynology: Principles and application* (Vol. 1, pp. 29–50). Salt Lake City, UT: Publishers Press.
- Wu, K., Guo, J., Yao, W., Liu, Q., Liu, Y., & Liu, B. (2019). Analysis on the structure and accumulation differences of Hongche Fault Belt in Junggar Basin. *Geology and Resources*, 28(1), 57–65.
- Wu, K., Liu, B., Liu, Y., Jia, C., Guo, J., & Li, S. (2017). Characteristics, formation and evolution of fault system in Zhongguai Uplift of Junggar Basin, China. *Journal of Earth Sciences and Environment*, 39(3), 406–418.
- Yuan, R., Yang, B., Pan, C., Xuguang, G., Liliang, H., Wenjun, H., ... Zhao, K. (2020). Conglomerate petrology characterization using high-definition borehole electrical images in the Upper Urho Formation at Well JL42, Zhongguai Uplift, Junggar Basin, China. *Interpretation*, 8(3), 1–41.
- Zeck, H. P., & Williams, I. S. (2002). Inherited and magmatic zircon from Neogene Hoyazo Cordierite Dacite, SE Spain – Anatectic source rock provenance and magmatic evolution: In memoriam professor Chris Powell,† 2001.07. 21. *Journal of Petrology*, 43(6), 1089–1104.

- Zhang, G., Jin, L., Lan, L., & Zhao, Z. (2015). Analysis of the orderly distribution of oil and gas fields in China based on the theory of co-control of source and heat. *Natural Gas Industry B*, 2(1), 49–76.
- Zhang, X., Gao, F., Zhang, W., Yu, L., & Du, S. (2018). Fault characteristics and deformation process of Zhongguai Uplift in northwestern margin of Junggar Basin. *Science Technology and Engineering*, 18(10), 6–11.
- Zhang, Z., & Wu, S. (1991). Chapter 6 Permian in *The Palaeozoic Erathem of Xinjiang* (pp. 329–481). China: Xinjiang Peoples's Publishing House Urumqi.
- Zhou, Y. (1994). Earliest pollen-dominated microfloras from the early Late Carboniferous of the Tian Shan Mountains, NW China: Their significance for the origin of conifers and palaeophytogeography. *Review of Palaeobotany and Palynology*, 81(2–4), 193–211.

How to cite this article: Shi, T., Li, Q., Amuti, A., Xiao, J., Liu, F., Yang, W., Li, Q., Zhang, H., Lü, Z., & Peng, H. (2021). Bashkirian taeniate bisaccate pollen-dominated palynological assemblage from northwestern Junggar Basin, Xinjiang

Province, China. *Geological Journal*, 1–12. <https://doi.org/10.1002/gj.4167>